

Three-dimensional imaging interferometric synthetic aperture lidar

Zhilong Zhao (赵志龙)^{1,2}, Jin Wu (吴谨)^{1*}, Yuanyuan Su (苏园园)^{1,2},
Na Liang (梁娜)^{1,2}, and Hongcheng Duan (段洪成)^{1,2}

¹*Institute of Electronics, Chinese Academy of Sciences, Beijing 100190, China*

²*University of Chinese Academy of Sciences, Beijing 100049, China*

*Corresponding author: jwu909@263.net

Received April 7, 2014; accepted June 3, 2014; posted online August 22, 2014

A monostatic strip-map mode interferometric synthetic aperture lidar (SAL) is reported. Using a chirped laser of about 5 mW at 1550 nm wavelength as the illumination source and two cross-track receiving apertures with a baseline of 1.6 mm, the lidar can generate both well-focused two-dimensional SAL images without adopting phase error removing techniques and three-dimensional images by interferometric SAL techniques. Detailed results are illustrated for retro-reflective or diffusive targets at a distance of 2.4 m.

OCIS codes: 110.6880, 280.4788, 280.3640, 110.0110.

doi: 10.3788/COL201412.091101.

Synthetic aperture lidar (SAL), being capable of imaging long distance objects in relatively short synthetic aperture time with high resolution, has been progressed greatly in recent years^[1–10]. With the advancement of SAL techniques, the potential three-dimensional (3D) imaging capability of SAL is drawing the attention of lidar researchers. The US Defense Advanced Research Projects Agency declared the realization of compelling 3D SAL imagery of extended diffuse targets on airplane platforms^[11]. An interferometric SAL (InSAL) was reported by the Spectrum Lab and Department of Physics in Montana State University (MSU) utilizing ultra-broad bandwidth actively linearized chirp laser centered at 1550 nm wavelength and about 200 mW power^[12]. So far, the 3D InSAL images provided by MSU is the only result demonstrated in public.

In the MSU setup, the detector could receive only one photon from each resolution pixel during a pulse, which will put forward high requirement on the sensitivity of the detector. In this letter, a monostatic InSAL in strip-map mode is reported, where, real lenses, instead of the tiny tip face of a single-mode fiber in the MSU setup, are used as the transmitting/receiving (T/R) apertures, enabling much less laser illuminating power (5 mW) in lidar operation. A simple photometric budget can be done like this: The laser beam with 5 mW transmitting power and 3 mrad divergence angle will irradiate 3×10^{13} photons/s on each 200×200 (μm) resolution pixel of the target 2.4 m away. And assuming the photons is back-scattered into a 2π solid angle, then each 0.4×0.4 (mm) lens will receive 1.32×10^4 photons from each resolution pixel within the actually used pulse duration of 100 ms. Moreover, the system can generate high-resolution two-dimensional (2D) images by straightforwardly following standard SAL image formation theory and not requiring phase error removing techniques as phase gradient autofocus (PGA)^[13].

Detailed results on the system description, phase history data (PHD) and 2D/3D images are illustrated.

The schematic of the monostatic strip-map mode InSAL is shown in Fig. 1. A chirped laser with power of about 5 mW is used as the illuminating source which provides a wavelength modulation range of 40 nm around 1550 nm. The wavelength scanning speed is 100 nm/s. Four signal recording channels are set in the system: Channel 1 monitors the absorption spectrum of a HCN cell to provide accurate frequency reference for different shots in the whole collection time; Channel 2 is the reference heterodyne signal for removing the frequency chirping nonlinearity in both Channels 3 and 4 by sharpness algorithm^[2]; Channels 3 and 4 record the heterodyne signals from the two cross-track apertures. The two cross-track apertures behind the receiving telescope with 10 times magnification are vertically set with 16 mm apart, forming a 1.6 mm baseline for InSAL imaging. The target is placed on a slant plane, which can be moved across the laser beam by a translational stage.

This monostatic strip-map mode InSAL is developed from a previous SAL setup in our laboratory^[14–16]. Two cross-track apertures are adopted in the receiving optics for InSAL configuration. Due to the excellent performance of the SAL setup, data from either Channel 3 or 4 in the InSAL could generate well-focused high-resolution images, usually referred to as the main and slave complex SAL images in InSAL terminology, just by following standard SAL image formation theory and not requiring any phase error removing techniques as PGA.

The interferometric phase of the two SAL images formed by the two cross-track apertures in this InSAL setup can be expressed as

$$\phi_{\text{inf}}(\mathbf{x}', f_r) = -2 \left[\frac{B(y_0 \sin \Phi - z_0 \cos \Phi)}{\lambda_0 L_0} \right], \quad (1)$$

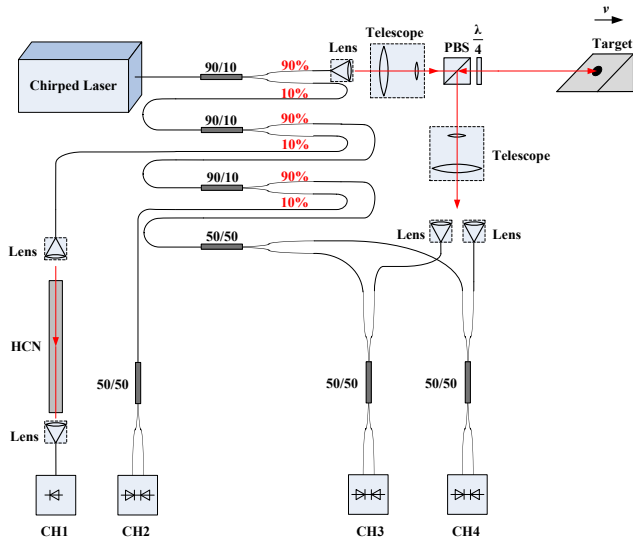


Fig. 1. Schematic of the monostatic strip-map InSAL.

where x' and f_r are coordinate values in azimuth (along-track) axis and range (cross-track) axis of the SAL image, B , L_0 , λ_0 , and Φ are baseline length, target distance, laser central wavelength, and side-looking angle, respectively, and y_0 and z_0 are coordinate values in the range and elevation directions, respectively. The variable z_0 is exactly the elevation information to be found out. And the term “ $-2\pi B y_0 \sin\phi / \lambda_0 L_0$ ” will cause the fringes in the interferogram, which are usually called “flat effect” in InSAL, and should be removed before 2D phase unwrapping.

The InSAL signal processing is shown in Fig. 2.

Step I: Form 2D complex SAL images. The main and slave complex SAL images are generated from the raw SAL data of the two cross-track apertures by standard SAL image formation theory: Fourier transformation for range compression and matched filtering for azimuth focusing.

Step II: Carry out image registration to maximize the coherence of the two SAL images. Generally, both pixel level registration and co-registration are required. In this monostatic InSAL, data are collected by a short baseline in a single pass, so a pixel level registration is adequate and co-registration is not used for getting a clear interferogram of the two SAL images due to the fine coherence in the system.

Step III: Multiply the main complex SAL image by the conjugate of the slave complex SAL image, and calculate the phase angle of the product to form the interferogram of the two SAL images.

Step IV: Remove the “flat effect” fringes from the interferogram. Removing the fringes will generate accurate target elevation information.

Step V: Mask and noise filtering. Select the area of interest in the 2D SAL image, and mask the corresponding area in the interferogram. Make 2D noise filtering to the masked interferogram.

Step VI: Get height profile of the target. Use 2D phase unwrapping to recover the elevation information

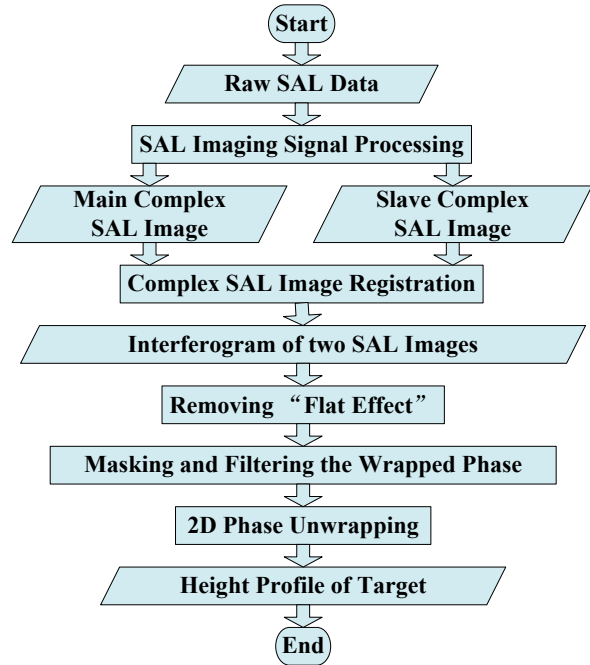


Fig. 2. Flow chart of InSAL signal processing.

from the noise filtered interferogram. In the 2D phase unwrapping process, the method of the least square and the network flow^[17,18] are both tried and found to be robust and helpful. However, the InSAL imaging results acquired by the method of the network flow seem more consistent with the actual target. Therefore, the method of the network flow is adopted in this work.

The target distance for 2D/3D imaging is about 2.4 m. With this distance, both cross-track apertures could generate well-focused SAL images with a high 2D special resolution which is very close to the theoretical azimuth resolution of $233 \mu\text{m}$ by synthetic aperture length of 8 mm and theoretical range resolution of $170 \mu\text{m}$ by heterodyne signal pulse length of 100 ms^[15,16], which is much higher than the fundamental limit resolution of 9.3 mm due to the real aperture size of 0.4 mm ($\sim \lambda_0 L_0 / D$); every elevation of 3.3 mm in the target will cause an interferometric phase shift of 2π according to Eq. (1).

Figure 3 shows the InSAL result of a ridge-shaped target. Figure 3(a) shows the photograph of the target, which is made of retro-reflective material and sticks on a ridge-shaped support made of thin steel plate. The total elevation of this retro-reflector target is about 2.5 mm. Figure 3(b) shows the main and slave SAL images formed in Step I, where the surface details, for instance, the “X”-shaped area of the target, are clearly displayed due to the well performance of the system. Figure 3(c) shows the interferogram right after image registration, where the dense “flat effect” fringes could be clearly seen. Figure 3(d) shows the wrapped phase obtained from Fig. 3(c) after removing “flat effect” fringes and noise filtering. Figure 3(e) shows the unwrapped phase from Fig. 3(d), which contains the

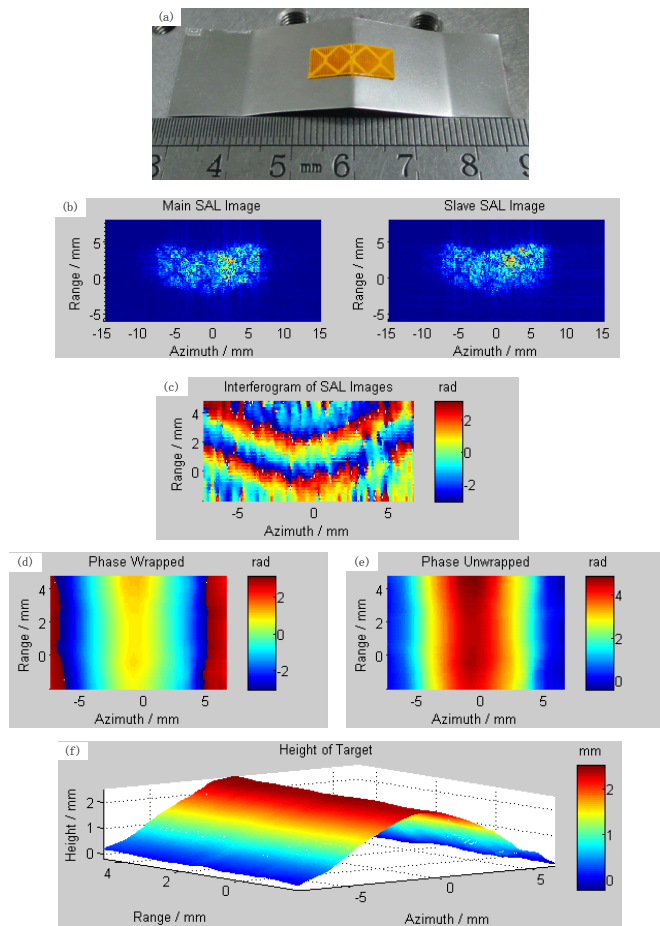


Fig. 3. Result of a retro-reflective target: (a) photograph of the target, (b) 2D SAL images, (c) interferogram of SAL images, (d) wrapped phase, (e) unwrapped phase, and (f) 3D InSAL image.

elevation information of the target. Figure 3(f) shows the reconstructed height profile of the target. From Fig. 3(f), the height of the ridge is 2.5 mm, which is well consistent with the 2.5 mm target shown in Fig. 3(a).

Figure 4 shows the InSAL result of a drawing pin. Figure 4(a) shows the photographs of the target, where the left photograph shows the pin on the stage and the right one shows the surface details of the pin. The smooth metal surface of the drawing pin is made rough by sandpaper to form diffusive backscattering to the laser light. Figure 4(b) shows the 2D SAL images and Fig. 4(c) shows the interferogram after image registration, where the dense “flat effect” fringes could be clearly seen. Figure 4(d) shows the wrapped phase obtained from Fig. 4(c) after removing “flat effect” fringes and noise filtering. Figure 4(e) shows the unwrapped phase from Fig. 4(d), which contains the elevation information of the target. Figure 4(f) is the reconstructed 3D InSAL image, showing the spherical shape of the target.

Figures 3 and 4 are the InSAL results of different targets. In Fig. 3, the strong backscattering target results in well-focused 2D images with details. In Fig. 4, the

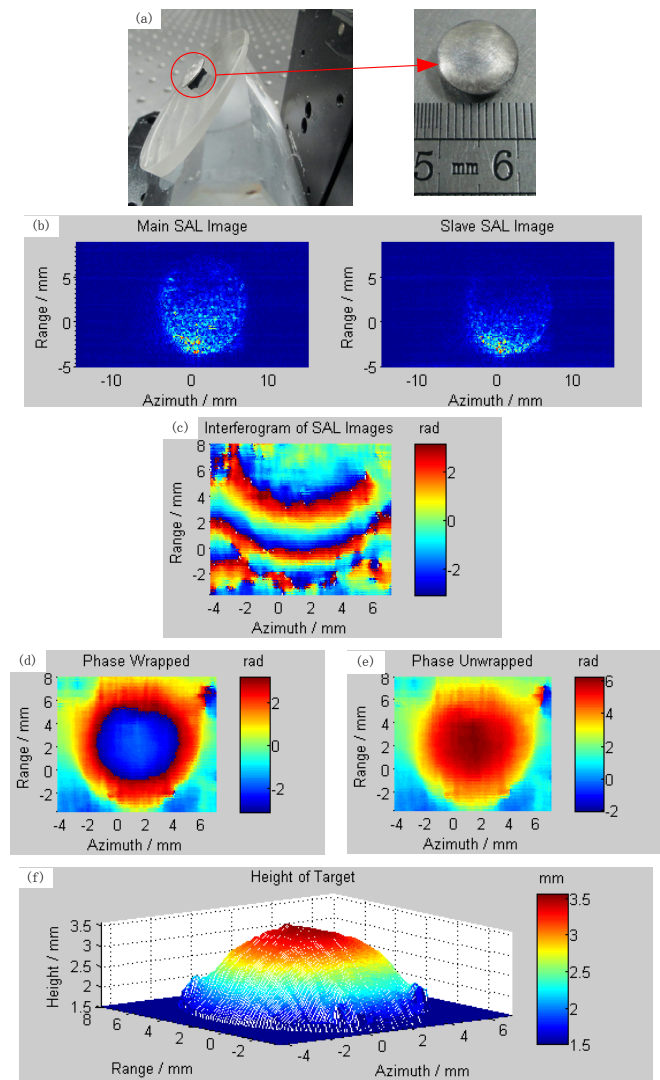


Fig. 4. Result of a diffusive target: (a) photographs of the target, (b) 2D SAL images, (c) interferogram of SAL images, (d) wrapped phase, (e) unwrapped phase, and (f) 3D InSAL image.

poor reflecting diffusive target leads to 2D images with inhomogeneous backscattering. However, in both cases, the 3D images are well reconstructed by InSAL technique.

Figure 5 shows the InSAL imaging result of a more complicated target made of three drawing pins. Figure 5(a) shows the photograph of the target and Fig. 5(b) shows the elevation profile of the three drawing pins obtained by InSAL processing, where the spherical shapes of the pins are clearly displayed. What should be mentioned in particular is that, the rough metal targets (drawing pins) are stuck to the rubber, and then placed on the board. The elasticity of the rubber makes it hard to keep a strictly certain angle of every drawing pins, and this makes these three thumbtacks look a bit different.

In conclusion, a monostatic InSAL in strip-map mode is successfully introduced. The well-performed system, using

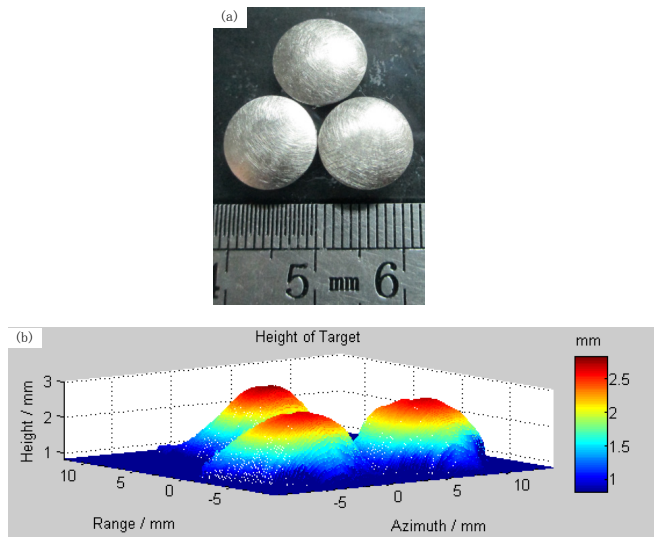


Fig. 5. Result of three drawing pins: (a) photograph of the target and (b) 3D InSAL image.

1550 nm wavelength chirped laser with power of about 5 mW as the illuminating source and real lenses as the T/R apertures, can maintain stable PHD and form high-resolution 2D SAL images and 3D InSAL images by straightforwardly following InSAL image formation theory and not adopting phase error removing techniques as PGA. Detailed 2D and 3D imaging results on both retro-reflective and diffusive targets in distance of about 2.4 m are given. To the best of our knowledge, this is the first time that a 3D imaging monostatic InSAL is reported with PGA-independent well-focused images.

As a high-resolution 3D imagery tool, InSAL may have a good prospect for remote sensing application, although there are still many technical challenges in developing a practical InSAL for outdoor uses, since enormous phase errors may be produced by mechanical vibration, atmosphere turbulence, etc^[19,20]. However, the difficulties in the complex outdoor condition can be overcome by adopting the increasingly mature technology of system controlling and signal processing.

This work was supported by the National “863” Project of China (No. 2007AA12Z107) and the National Natural Science Foundation of China (No. 61178071).

References

- 1 M. Bashkansky, R. L. Lucke, and E. Funk, *Opt. Lett.* **27**, 1983 (2002).
- 2 S. M. Beck, J. R. Buck, W. F. Buell, R. P. Dickinson, D. A. Kozlowski, N. J. Marechal, and T. J. Wright, *Appl. Opt.* **44**, 7621 (2005).
- 3 E. A. Stappaerts and E. T. Scharlemann, *Opt. Lett.* **30**, 2385 (2005).
- 4 B. D. Duncan and M. P. Dierking, *Appl. Opt.* **48**, 1168 (2009).
- 5 J. R. Buck, B. W. Krause, A. I. R. Malm, and C. M. Ryan, in *Proceedings of CLEO 2009 PThB3* (2009).
- 6 B. W. Krause, J. Buck, C. Ryan, D. Hwang, P. Kondratko, A. Malm, A. Gleason, and S. Ashby, in *Proceedings of CLEO 2011 PDPB7* (2011).
- 7 S. Turbide, L. Marchese, M. Terroux, F. Babin, and A. Bergeron, *Proc. SPIE* **8542**, 854213 (2012).
- 8 H. Jiang, J. Zhao, and J. Di, *Chin. Opt. Lett.* **10**, 090901 (2012).
- 9 Y. Yan, J. Sun, X. Jin, Y. Zhou, Y. Zhi, and L. Liu, *Chin. Opt. Lett.* **10**, 091101 (2012).
- 10 L. Liu, *Appl. Opt.* **52**, 579 (2013).
- 11 J. Ricklin, B. Schumm, and M. Dierking, AFRL-RY-WP-TP-2010-1063 (2007).
- 12 S. Crough and Z. W. Barber, *Opt. Exp.* **20**, 24237 (2012).
- 13 P. H. Eichel, D. E. Wahl, D. C. Ghiglia, and C. V. Jakowatz, *IEEE Trans. Aerosp. Electron. Syst.* **30**, 827 (1994).
- 14 J. Wu, Z. Yang, Z. Zhao, F. Li, D. Wang, Y. Tang, Y. Su, and N. Liang, *J. Infrared Millim. Waves* **32**, 514 (2013).
- 15 J. Wu, F. Li, Z. Zhao, Z. Yang, D. Wang, Y. Tang, Y. Su, and N. Liang, in *Proceedings of the 5th International Symposium on Photoelectronic Detection and Imaging* (2013).
- 16 Z. Yang, J. Wu, Z. Zhao, D. Wang, Y. Su, and N. Liang, *Front. Optoelectron.* **6**, 251 (2013).
- 17 D. C. Ghiglia and M. D. Pritt, *Two-Dimensional Phase Unwrapping: Theory, Algorithms, and Software* (Wiley-Interscience, 1998).
- 18 M. Costantini, *IEEE Trans. Geosci. Remote Sensing* **36**, 813 (1998).
- 19 T. J. Karr, *IEEE Trans. Antenn. Propag.* **55**, 1122 (2007).
- 20 G. Hong and L. Guo, *J. Infrared Millim. Waves* **30**, 571 (2011).